

Article

A Study on the Formation Process of Fe Clusters During Insulation of Cu₉₅Fe₅ Alloy

Xufeng Wang, Hanyu Zhang, Congjing Xu, Xufeng Gao, Zhenhao Zhang, Yungang Li * and Lu Liu *

College of Metallurgy and Energy, North China University of Science and Technology, Tangshan 063210, China; wangxf@ncst.edu.cn (X.W.); 15631867824@163.com (H.Z.); lucky20182024@163.com (C.X.); gaoxf2025@163.com (X.G.); 13053334352@163.com (Z.Z.)

* Correspondence: lyg@ncst.edu.cn (Y.L.); liulu@ncst.edu.cn (L.L.)

Abstract: The molecular dynamics simulation technique was utilized to examine the structural variations of the Cu₉₅Fe₅ alloy, as well as the precipitation and aggregation processes of Fe atoms during heat preservation. It is shown that the crystallization temperature of the Cu₉₅Fe₅ alloy under the condition of a 2×10^{10} K/s cooling rate is 882 K. Crystallization of the alloy occurs when it is insulated under the temperature conditions of 900 K, 1000 K, and 1100 K. The lower the holding temperature, the shorter the holding time required for the system to initiate crystallization. In other words, lower temperature holding facilitates easier crystallization. The formation process of Fe clusters has been investigated. The size and quantity of Fe clusters at various stages are influenced by the interatomic interaction forces between Fe atoms, the diffusion capabilities of Fe atoms, the local structural rearrangement of nondispersive atoms, and the interfacial energy between Fe clusters and the Cu matrix. The formation of Fe clusters in the insulation process mainly undergoes four stages: First, the initial small clusters are disassembled under the influence of molecular thermal motion and the attractive interactions between Fe atoms. This process leads to the formation and growth of new small clusters. Secondly, the clusters condense and grow under non-diffusive atomic local structure rearrangement. Third, the Fe clusters are sphericalized under Cu-Fe interfacial energy. Fourth, individual Fe atoms are diffused into large Fe clusters under the action of molecular thermal motion.

Keywords: Cu-Fe alloy; heat preservation; crystallization temperature; Fe clusters



Academic Editor: Jia Huo

Received: 21 January 2025

Revised: 10 February 2025

Accepted: 13 February 2025

Published: 16 February 2025

Citation: Wang, X.; Zhang, H.; Xu, C.; Gao, X.; Zhang, Z.; Li, Y.; Liu, L. A Study on the Formation Process of Fe Clusters During Insulation of Cu₉₅Fe₅ Alloy. *Processes* **2025**, *13*, 557. <https://doi.org/10.3390/pr13020557>

Copyright: © 2025 by the authors. Licensee MDPI, Basel, Switzerland. This article is an open access article distributed under the terms and conditions of the Creative Commons Attribution (CC BY) license (<https://creativecommons.org/licenses/by/4.0/>).

1. Introduction

Copper-iron (Cu-Fe) alloys offer several advantages, including low cost and an abundance of raw materials. These alloys also exhibit remarkable magnetoresistance effects and unique physical properties. Consequently, they have found extensive applications in various fields, such as electronics, aerospace, and automotive industries [1–4]. According to the analysis of the Cu-Fe equilibrium phase diagram, Fe atoms are more solidly soluble in Cu at high temperatures, and Fe is almost insoluble in Cu at low temperatures. Under non-equilibrium solidification conditions, iron (Fe) atoms will be directly dissolved into the copper (Cu) matrix, resulting in the formation of a supersaturated Cu-based solid solution. The presence of these supersaturated Fe atoms leads to significant impurity scattering, which can severely impair the electrical conductivity of the composites [5,6]. Many scholars use a fast solidification method at this stage to obtain a Cu-based solid solution with a uniform distribution of Fe atoms. They then precipitate Fe dissolved in the Cu matrix via high-temperature aging to obtain both mechanical and electrical conductivity of the Cu-Fe alloy [1,7,8]. It can be seen that the crystal structure of the Cu matrix and the

distribution state of Fe atoms in the matrix are the key factors affecting the properties of the alloy. Molecular dynamics (MD) simulation has emerged as a crucial methodology for investigating the atomic-scale evolution of microstructural and crystallographic features in alloys subjected to thermal processing. This computational approach facilitates a systematic exploration of short-range order (SRO)-driven local structural rearrangements during heat treatment while providing fundamental mechanistic insights that inform the rational design and optimization of advanced metallic materials [9]. A. Samiri et al. employed molecular dynamics simulations to investigate the structural and dynamic properties of various binary alloys throughout the cooling process [10]. Furthermore, in conjunction with the kinetics of alloy solidification, the structural transformations and growth patterns of the alloy during the solidification process were elucidated. Additionally, the mechanisms underlying phase formation and defect generation throughout the alloy solidification process were revealed [11]. The authors used molecular dynamics methods to study the structural changes and Fe precipitation process of the Cu₁₀₀-XFeX (X = 1%, 3%, 5%) alloy under the conditions of the cooling rates of 1×10^{13} K/s, 2×10^{12} K/s, 2×10^{11} K/s, and 2×10^{10} K/s [12,13]. The alloy begins to experience substantial aggregation of Fe atoms at temperatures exceeding 200 K above the crystallization point. It can be seen that the formation of Fe clusters is influenced by the cooling rate and the Fe content in the system. This is crucial for studying Copper–iron alloys during preparation, heat treatment, or service. Although the phenomenon of Fe cluster formation has been initially described, along with the reduction in temperature during the solidification process of alloy systems, several aspects remain unclear. These include the formation mechanism of Fe clusters during solidification, the manner in which Fe clusters undergo crystalline transformation, and how insulation temperature affects the morphology of these clusters. Therefore, it is essential to investigate the behavior of Fe atoms under varying heat preservation temperatures. This study aims to provide a theoretical foundation for understanding Cu-Fe alloys with rich Fe phase macro-control and enhanced treatment methods. Therefore, there is an urgent need to study the behavior of Fe atoms during the holding process at different temperatures, to provide a theoretical basis for the macro-control and improvement of Fe-rich phases in Cu-Fe alloy.

In this study, molecular dynamics simulation methods are employed to investigate the holding process of the Cu₉₅Fe₅ alloy at varying temperatures. The research aims to examine the impact of the holding process on the alloy's crystal structure and the precipitation behavior of Fe atoms. Additionally, it seeks to explore the mechanisms underlying Fe atom precipitation under different temperature-holding conditions. Through these simulation studies, a theoretical foundation is provided for both laboratory research and industrial production.

2. Simulation Methods

According to the study, the Cu-Fe alloy was first modeled using AtomsK (The version number of AtomsK is Pierre Hirel 2010- Version 0.11) [14] software (the Swiss-army knife of atomic simulations). Specifically, it is the first established Cu single cell; the single cell is replicated as a $30 \times 30 \times 12$ supercell. At this time, the simulation box contains 43,200 Cu atoms, and then, the Cu atoms in the box are randomly replaced with 2160 Fe atoms to obtain the alloy model required for the simulation. Subsequently, a molecular dynamics approach was used for the simulation study, and the simulation calculations were implemented using LAMMPS (the large-scale atomic/molecular massively parallel simulator), a large-scale atomic/molecular simulator designed and developed by Sandia National Laboratory, Albuquerque, NM, USA [15]. The interaction potential function developed by Bonny et al. [16] was chosen for the simulation, which is a system of potential

functions that has been often used to study the phase separation process of Fe-Cu alloys in the past few years and can accurately describe the process of Fe atom precipitation in Cu-Fe alloys. All the steps in the molecular dynamics simulation were performed using the NPT system, and the time step was chosen as 2 fs. The system pressure was maintained at 0 Bar, and the control of pressure was executed using a Nose–Hoover algorithm. The simulation was performed using periodic boundary conditions. The model was first run at 2200 K for 300,000 time steps to fully diffuse the atoms, and then, the alloy was cooled to 1400 K, 1300 K, 1200 K, 1100 K, 1000 K, 900 K, 800 K, and 500 K under the 2×10^{10} K/s cooling-rate condition; held at this temperature for 140 ns; subsequently cooled from the holding temperature condition to 300 K under 2×10^{10} K/s cooling-rate condition; and cooled from the holding temperature condition to 300 K. Structural information and kinetic and thermodynamic parameters of the system are recorded during the simulated cooling of the alloy. Finally, OVITO visualization software (The version number of OVITO is 3.8.3.) [17] was used to visualize the simulation results, and methods, such as common neighbor analysis and cluster analysis, were used to analyze the crystal microstructure and Fe cluster formation and growth patterns during the simulation process [18,19].

3. Results and Discussion

3.1. Structural Changes in the System of the Alloy Cooling–Insulation Process

The system atomic potential energy versus temperature change curve can truly and objectively reflect the microstructural changes in the alloy system during the cooling process [20,21]. It can simply and intuitively analyze the system's phase transition process. In general, the alloy melts in the continuous cooling process. If the curve deviates from the straight line without mutation, the alloy system will form amorphously. A linear regression was applied to the curve, with the intersection of the two fitted lines representing the crystallization point. When the curve exhibits a deviation from linearity and experiences a sudden change, it indicates that a crystal has formed; thus, this point of abrupt change is identified as the crystallization point [22,23].

The curves of the atomic potential energy of the system versus the temperature change during alloy solidification (without holding) of the Cu95Fe5 alloy under the condition of the 2×10^{10} K/s cooling rate are plotted as shown in Figure 1.

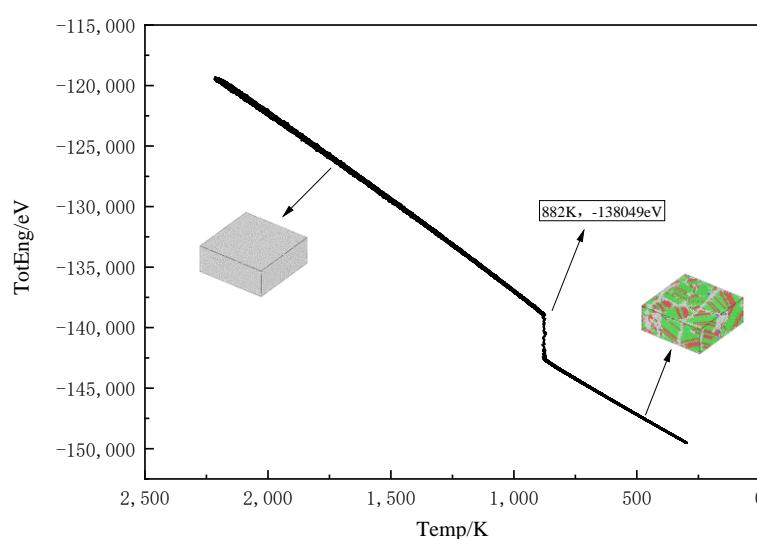


Figure 1. Atomic potential energy–temperature variation line during solidification of Cu95Fe5 alloy.

As the temperature of the system decreases, the intensity of thermal vibrations among the atoms gradually diminishes, leading to a corresponding reduction in their velocity.

These changes facilitate the combination of atoms into an ordered structure. The formation of this ordered structure results in a decrease in the volume of the system. Furthermore, this reduction in volume, along with alterations in atomic positions, contributes to a decrease in the overall energy of the system. When the system volume is lowered to a specific level, the system's energy is minimized, leading to the rapid dissolution of the formed alloy cluster structure. The atoms then re-combine into a more stable arrangement, resulting in crystallization. This process is marked by a sudden decrease in the system's energy, reflected in a noticeable change in the atomic potential energy–temperature curve. The gray color in Figure 1 indicates the other category (not belonging to any common crystal category), the green crystal type is FCC, the blue crystal type is BCC, and the red crystal type is HCP. Crystallization of the melt occurs when the alloy is at a temperature of 882 K. The melt is liquid above 882 K and solid below it [24,25].

After previous studies, it has been found that the alloy temperature during alloy solidification has an important effect on the formation of Fe clusters. The alloy model was first run at 2200 K for 300,000-time steps to allow full diffusion of atoms. Then, the alloy was cooled to 1400 K, 1300 K, 1200 K, 1100 K, 1000 K, 900 K, 800 K, and 500 K under 2×10^{10} K/s cold rate condition, held at this temperature for 140 ns, and subsequently cooled to 300 K under the 2×10^{10} K/s cooling-speed condition from the holding temperature condition to 300 K. The atomic potential energy–temperature variation line during the solidification of the Cu95Fe5 alloy was plotted as shown in Figure 2.

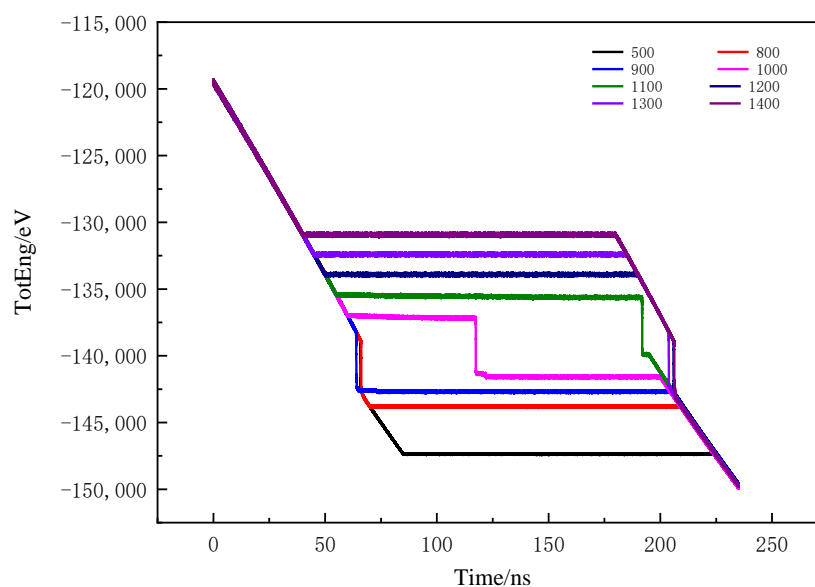


Figure 2. Atomic potential energy–temperature variation line during solidification of Cu95Fe5 alloy (including holding at different temperatures for 140 ns).

According to the analysis of the graph line changes, the alloy is in a crystalline state before it is held at 500 K and 800 K. The atomic potential energy–temperature change line remained straight during the 500 K and 800 K temperature holding, which indicates that there was no significant change in the alloy structure from a macroscopic point of view. At the end of the holding period, the atomic potential energy continues to decrease with temperature. This result shows that the volume of the alloy decreases, and the structure becomes denser during this process. The change curve of the insulation properties of the alloy system under 900 K temperature conditions was analyzed in detail. In the process of decreasing the temperature of the alloy, when the temperature of the system reaches 900 K, there is a rapid decrease in the atomic potential energy. This phenomenon indicates that the crystallization of the alloy occurs at 900 K. According to the analysis of Figure 1, under

the condition of the 2×10^{10} K/s cooling rate, the crystallization point of the Cu95Fe5 alloy should be 882 K. Under the insulation temperature of 900 K, the crystallization of the alloy occurs early in the insulation process. This observation suggests that high-temperature insulation can preliminarily increase the crystallization point of the alloy. The atomic potential energy change curves of the alloy at holding temperatures of 1000 K and 1100 K show that the system is in the liquid state before the start of the holding period, and during the holding period, it is clearly observed that there is a sudden change in the curves during the holding process, which indicates that the alloy is crystallized at this temperature. Comparing the conditions of the holding temperatures of 1000 K with those of 1100 K, the crystallization occurs in a shorter period at the holding temperature of 1000 K, which indicates that it is more likely to be crystallized at low temperatures. In the atomic potential energy–temperature change curves of the alloy system under the holding conditions of 1200 K, 1300 K, 1400 K, and 1500 K, the alloy has been a straight line without sudden change during the holding process of 140 ns. This indicates that the alloy has not crystallized under these conditions, and whether the internal structure of the alloy has been altered needs to be further investigated.

To further investigate the effect of the holding temperature on the alloy structure during the alloy-holding process, the crystal configuration was analyzed using the OVITO visualization software, (The version number of OVITO is 3.8.3.) as shown in Figure 3.

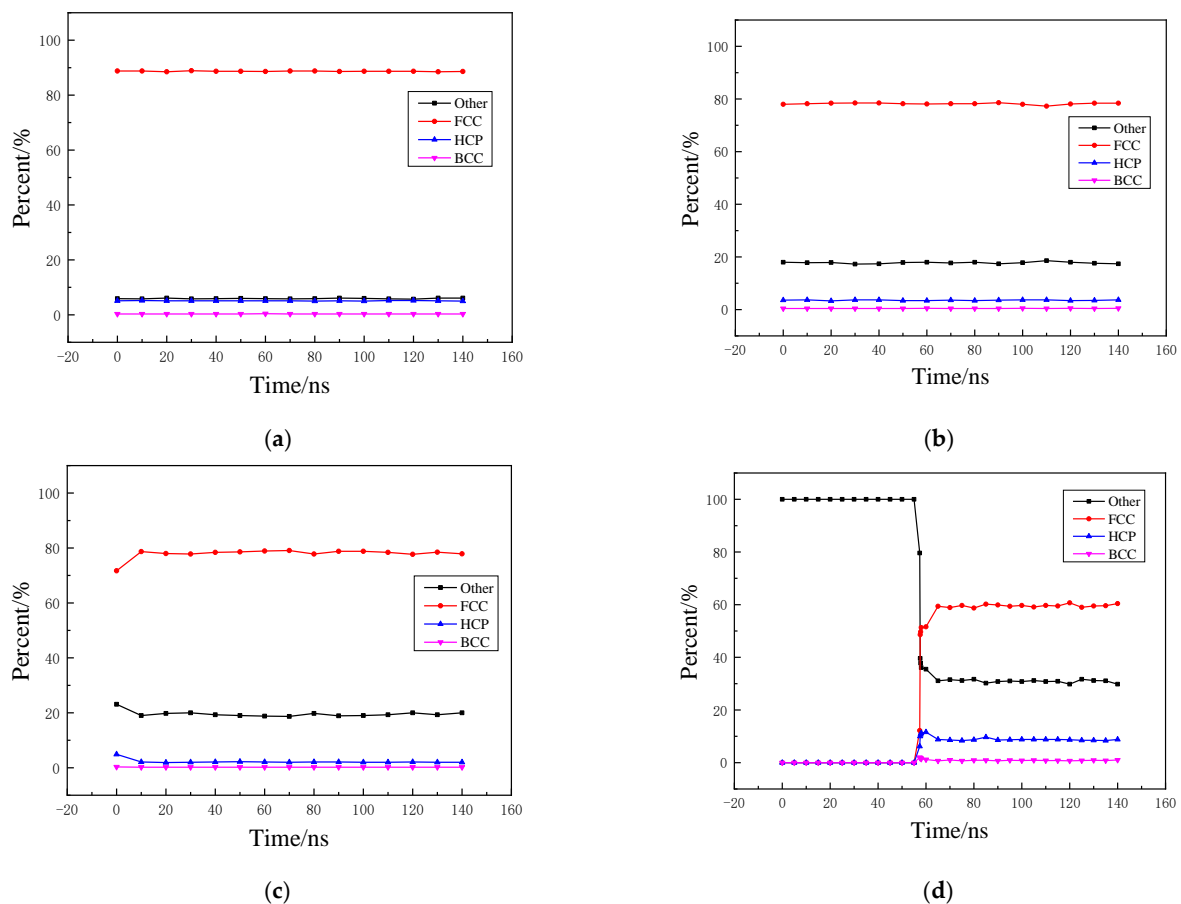


Figure 3. Cont.

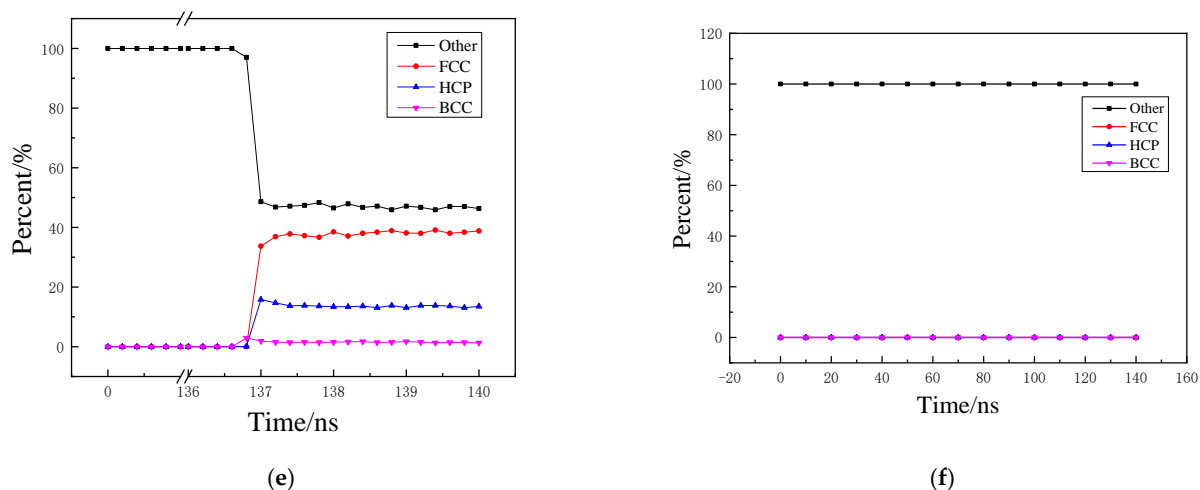


Figure 3. Analysis of crystal types during alloy holding: ((a): 500 K, (b): 800 K, (c): 900 K, (d): 1000 K, (e): 1100 K, (f): 1200 K).

The results are shown in Figure 3. The proportion of each type of crystal structure is basically unchanged when the alloy is held at 500 K and 800 K temperatures, which indicates that the structure of the alloy has not changed. The structure of the alloy system at 800 K thermal insulation is mainly that the other category represents atoms (not belonging to any crystal structure, which is generally considered to be defective and not on the lattice site) whose structures account for more. The sum of other crystal types, such as FCC, accounts for less. When the alloy was held at 900 K, the proportion of each type of crystal structure changed slightly for 5 ns at the beginning of the holding time and then remained essentially unchanged. Combined with the above analysis, the main reason for this phenomenon is that the alloy was held at a temperature (900 K) higher than the normal crystallization point (882 K), which increased the crystallization point of the alloy. The alloy crystallizes at 900 K. The alloy structure is unstable in the early crystallization stage, but subsequent heat preservation leads to a more stable alloy structure. When the alloy is held at temperatures of 1000 K and 1100 K, crystallization occurs during the holding process, transforming the alloy from a liquid to a solid. The liquid–solid transition takes less time at 1000 K. Figure 3d,e show that at the early stage of crystallization, the proportion of each crystal type in the system varies relatively greatly. Specifically, the proportions of HCP and BCC crystal structures show an increasing and then decreasing trend, the proportion of the other category represents atoms continues to decrease, and the crystal type of FCC structure continues to rise, which is because the alloy is a Cu matrix with a predominantly FCC structure, and the atom groups with non-FCC structures preferentially crystallize at the early stage of crystallization. For example, with Fe atoms dominating the BCC atom group, with the prolongation of the holding time, some of the atoms of the non-FCC structure of the atom group are redistributed, and some of the atoms are inlaid into the matrix of the FCC, so that the proportion of the FCC crystal structure type continues to increase. With the prolongation of the holding time, the alloy is gradually stabilized, and the proportion of each crystal structure type remains basically unchanged. From the alloy in 1000 K and 1100 K temperature conditions, the detailed processes of the changes in the insulation of the crystal structure and the insulation process of the internal alloy atom migration and aggregation need further study. When the alloy is held at 1200 K temperature, the alloy is always in a liquid state without crystallization within 140 ns holding time, and further study is needed to extend the holding time to see if the alloy will be crystallized. It is noteworthy that the percentage of the other category represents atoms in the alloy at the end of holding gradually increasing with the increase in holding temperature, which

indicates a decrease in the stability of the alloy. It is necessary to analyze the crystal types of the alloy after cooling (300 K). Figure 4 plots the scale of crystal types of the alloy when the temperature is reduced to 300 K after holding.

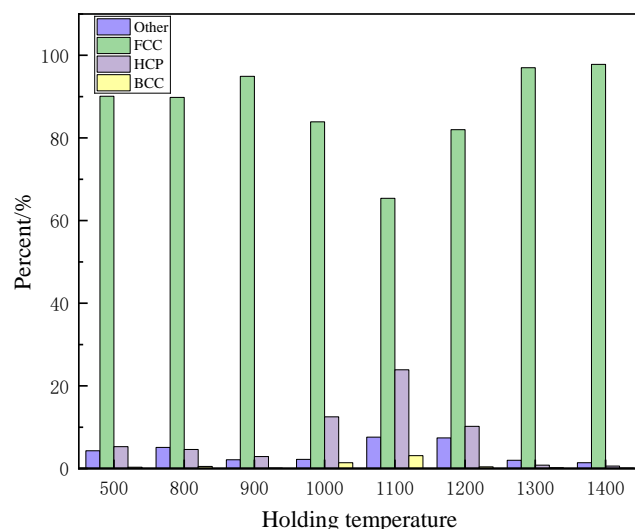


Figure 4. Scale diagram of alloy crystal types at 300 K.

Combining the data of Figure 3 and comparing them with Figure 4, it can be found that most of the other-type structures in the alloy are transformed into FCC, HCP, and BCC crystal structures after insulation, which again proves that the alloy is a non-stationary alloy and some atoms are not in the lattice sites during the insulation process. According to the modeling analysis, it can be seen that the alloy is a Cu alloy based on FCC, so it is more meaningful to study the effect of the holding temperature on the structure of the alloy when cooling down to 300 K via the change in the percentage of the FCC crystal type. As shown in the figure, the FCC crystal structure occupies the lowest percentage at 300 K after 1100 K insulation, which indicates that this insulation condition has the greatest influence on the structure of the alloy, and the migration and aggregation of atoms in the alloy are the most intense, followed by the conditions of the adjacent 1000 K and 1200 K insulation temperatures.

3.2. Study on the Precipitation Mechanism of Fe Clusters

3.2.1. Radial Distribution Function Analysis

The radial distribution function, which can be expressed as $g(r)$, is a statistical parameter that characterizes the distribution of atoms in a system. $g_{\alpha\beta}(r)$ physical significance is the ratio of the probability of finding atom β at a fixed atom α at a distance r from the radius relative to the conditional probability [26,27]. The radial distribution function can effectively give the atomic radius, atomic spacing, coordination number, and other structural information, which are used to distinguish liquid, crystalline, and amorphous. According to the law of change in the peak of the radial distribution function curve, it can judge the strength of inter-atomic interaction, short-medium-range ordering, and so on [28,29].

$$g_{\alpha\beta}(r) = \frac{L^3}{N_{\alpha}N_{\beta}} \left[\sum_{i=1}^{N_{\alpha}} N_{i\beta}(r) / (4\pi r^2 \Delta r) \right] \quad (1)$$

α and β denote the atomic classes, L denotes the side length of the simulation box, and N_{α} and N_{β} denote the number of α and β atoms, respectively, $N_{i\beta}(r)$ denotes the number of β atoms in the spherical shell from the i -th α atom r to $r + \Delta r$, and Δr denotes the thickness of the nuclear shell.

According to the previous study, the radial distribution function of Fe atoms during the solidification of Cu-Fe alloys is characterized by significant changes. The first peak of the radial distribution function indicates that the alloy is crystallized if it is a symmetric sharp peak; otherwise, it is a liquid phase in the molten state. The height of the peak represents the aggregation capacity of Fe atoms. As a result, the radial distribution function of Fe atoms in Cu-Fe alloys at different temperatures is plotted in Figure 5.

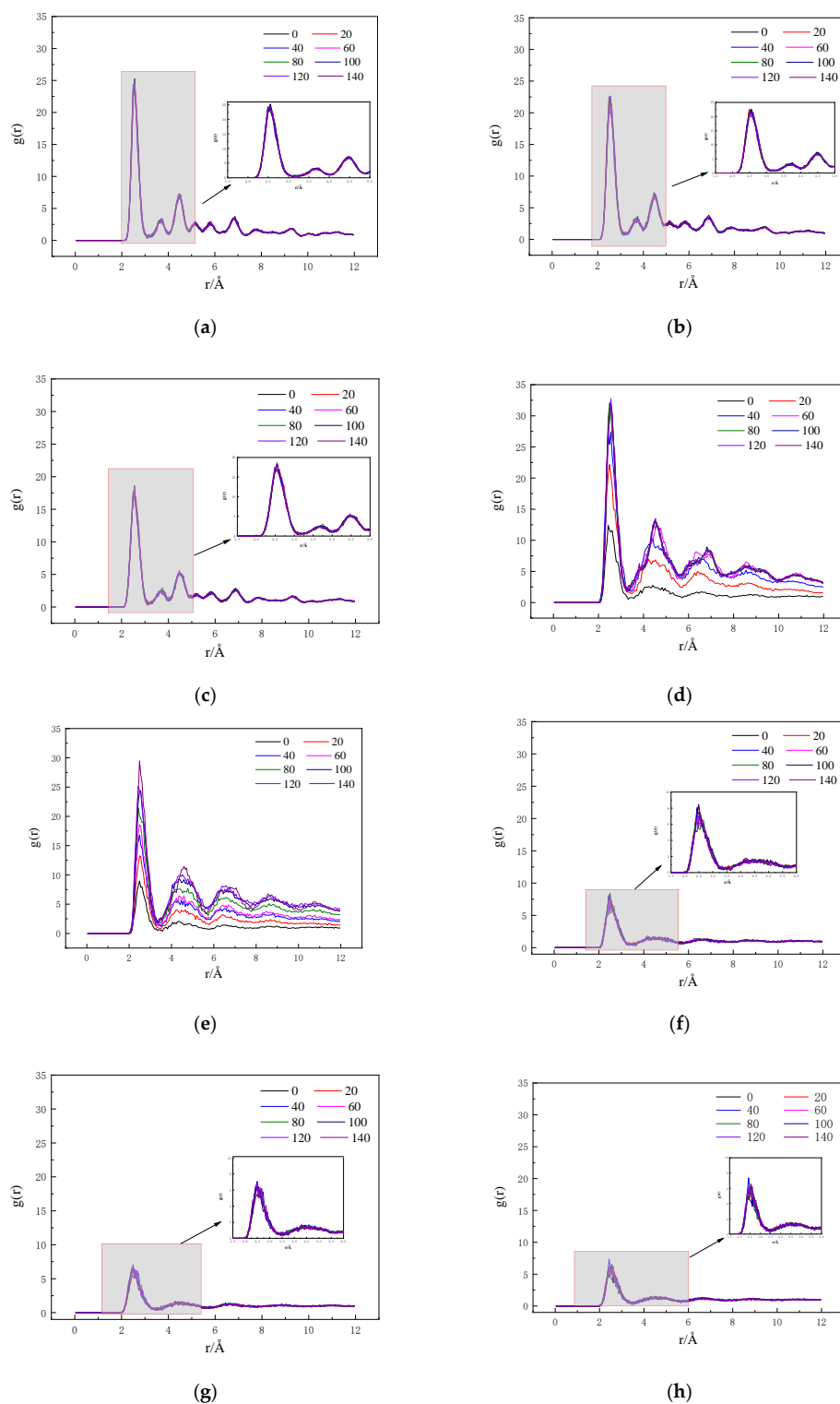


Figure 5. Radial distribution function of Fe atoms in alloys during holding at different temperatures ((a): 500 K, (b): 800 K, (c): 900 K, (d): 1000 K, (e): 1100 K, (f): 1200 K, (g): 1300 K, (h): 1400 K).

In Figure 5a–h represent the radial distribution function curves of the alloy at different times under 500 K, 800 K, 900 K, 1000 K, 1100 K, 1200 K, 1300 K, and 1400 K holding conditions, respectively. The radial distribution function curves at various times during the holding process exhibit significant overlap, as observed in Figure 5a–c. This finding indicates that the Fe atoms do not undergo migration and remain in a relatively stable state throughout the holding process. In addition, the first peaks of the curves are all symmetric sharp peaks, which again proves that the alloy is in a crystalline state at this temperature. The comparison of the highest values of the first peak in plots Figure 5a–c reveals a gradual decrease from Figure 5a–c. This trend indicates that the alloy exhibits the strongest interatomic forces and the most compact arrangement of Fe atoms when maintained under thermal conditions at 500 K. The changes observed in Figure 5d,e are more significant; as the insulation time increases, the radial distribution function of Fe atoms at the first peak also rises. This indicates that during this process, Fe atoms attract one another and gradually become aggregated. Comparing the Figure 5d,e, the first peak of the alloy reaches the highest value at 1000 K temperature with 60 ns holding time, while the first peak of the alloy reaches the highest value at 1100 K temperature with 140 ns holding time, which indicates that the low-temperature holding time is more favorable for the aggregation of Fe atoms. The first peak of the curve in Figure 5f does not show a clear high–low distribution, but there is still a high–low distribution trend. Combined with the Figure 5d,e curve graph trend and Figure 4 analysis, for the alloy in the 1200 K temperature-holding conditions, the Fe atoms still tend to aggregate. If the holding time continues to be prolonged, the Fe atoms will likely aggregate and crystallize. The peaks of the first peak in the curves of Figure 5g,h are not very different and are asymmetric, which indicates that the alloy is in a molten liquid state, and there is no tendency for the aggregation of Fe atoms.

3.2.2. Mean Square Displacement Analysis

Atomic diffusion is the process by which atoms move from one of their positions to another across lattice vacancies or other defect sites during thermal movement within a crystal [30]. In molecular dynamics simulations of alloy systems, the rate of atomic diffusion motion is described by the atomic diffusion coefficient, which is often achieved by counting the mean square displacements (MSDs) of the atoms during the simulation [31].

$$D^* = \lim_{t \rightarrow \infty} \frac{1}{2Nt} \langle |r(t) - r(0)|^2 \rangle \quad (2)$$

N—the dimension of the simulation system, N=3 for this system; t—the simulation time; ps, r(t), r(0)—the position of the atom at time t and the initial position of the atom, respectively.

$$MSD = \langle r^2(t) \rangle = \frac{1}{N} \sum_{i=1}^N \langle |r(t) - r(0)|^2 \rangle \quad (3)$$

where MSD is the mean square displacement.

Equations (1) and (2) yield the following:

$$D^* = \frac{MSD}{6t} \rightarrow MSD = 6D^*t \quad (4)$$

In total, 1/6 of the slope of the MSD vs. t curve is the diffusion coefficient of Fe atoms.

Figure 6 plots the MSD of Fe atoms extended in the X, Y, and Z directions versus the holding time of the alloy during holding at different temperature conditions.

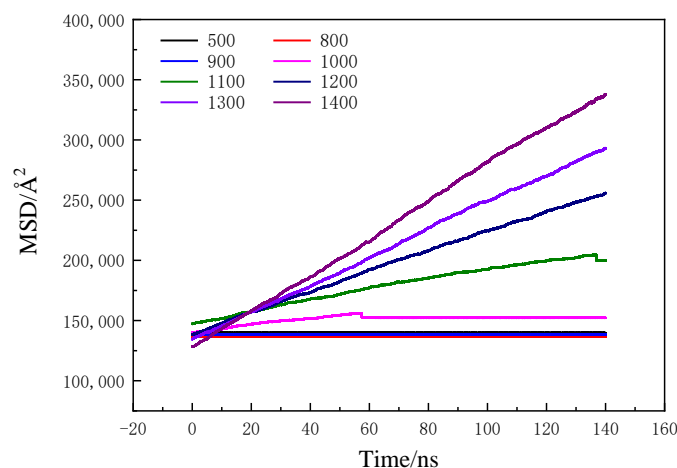


Figure 6. MSD of Fe atoms extended in X, Y, and Z directions versus holding time of the alloy during holding time at different temperatures.

When the alloy is held at 500 K, 800 K, and 900 K, the MSD and time curves are approximately parallel to the X-axis. From the above analysis, it can be seen that the alloy is in a crystalline state under this holding condition, and the MSD data show that there is almost no migration of Fe atoms within the crystal. The alloys were pre-insulated at 1000 K and 1100 K. The MSD data of the alloys increased with the increase in the holding time and then suddenly decreased at about 57 ns and 136 ns, respectively, after which they were approximately parallel to the X-axis. When the alloy is maintained at temperatures of 1200 K, 1300 K, and 1400 K, the relationship between MSD and time exhibits a nearly linear trend. Furthermore, the MSD values increase with prolonged holding duration. The diffusion coefficients of Fe atoms in the alloy at various holding temperatures are presented in Table 1. Calculated results indicate that as the insulation temperature increases, the diffusion coefficient of Fe atoms also rises. This observation suggests that temperature plays a crucial role in the diffusion process of Fe atoms. Furthermore, the enhancement of thermal movement among Fe atoms is attributable to the rise in insulation temperature. The diffusion coefficient of Fe atoms in the alloy system is negative when holding at 500 K, 800 K, and 900 K, which indicates that the diffusion of Fe atoms in this process is uphill diffusion. There is a tendency for Fe atoms to migrate from the low-concentration area to the high-concentration area, which is mainly manifested in the crystal structure change trend in conjunction with the above analysis. The diffusion coefficient of Fe atoms is the positive value when the alloy is held at temperatures above 1000 K, and the atomic diffusion is intense, but the radial distribution function data show that Fe atoms have a tendency to aggregate under the temperature conditions of 1000 K and 1100 K. In order to explain the reason for this, the aggregation behavior of Fe atoms is visualized and analyzed.

Table 1. Diffusion coefficients of Fe atoms in alloys at different holding temperatures.

Holding Temperature T (K)	D^* ($\text{cm}^2 \text{s}^{-1}$)
500	-4.5695×10^{-11}
800	-8.825×10^{-10}
900	-2.4938×10^{-9}
1000	4.6867×10^{-6} (0–57 ns)
1100	7.0698×10^{-6} (0–136 ns)
1200	1.3933×10^{-5}
1300	1.9081×10^{-5}
1400	2.5438×10^{-5}

3.2.3. Study of Fe Atom Precipitation Behavior During Solidification of Cu-Fe Alloys

The representative conditions under various insulation processes, specifically at temperatures of 800 K, 1000 K, 1200 K, and 1400 K (with time intervals of 0 ns, 30 ns, 60 ns, and 120 ns), were chosen to analyze the atomic distribution state of Fe for visualization purposes. Atomic visualization is realized by using the cluster analysis function of OVITO software, (The version number of OVITO is 3.8.3.) and different colors in the picture represent clusters containing different numbers of atoms, as in Figure 7.

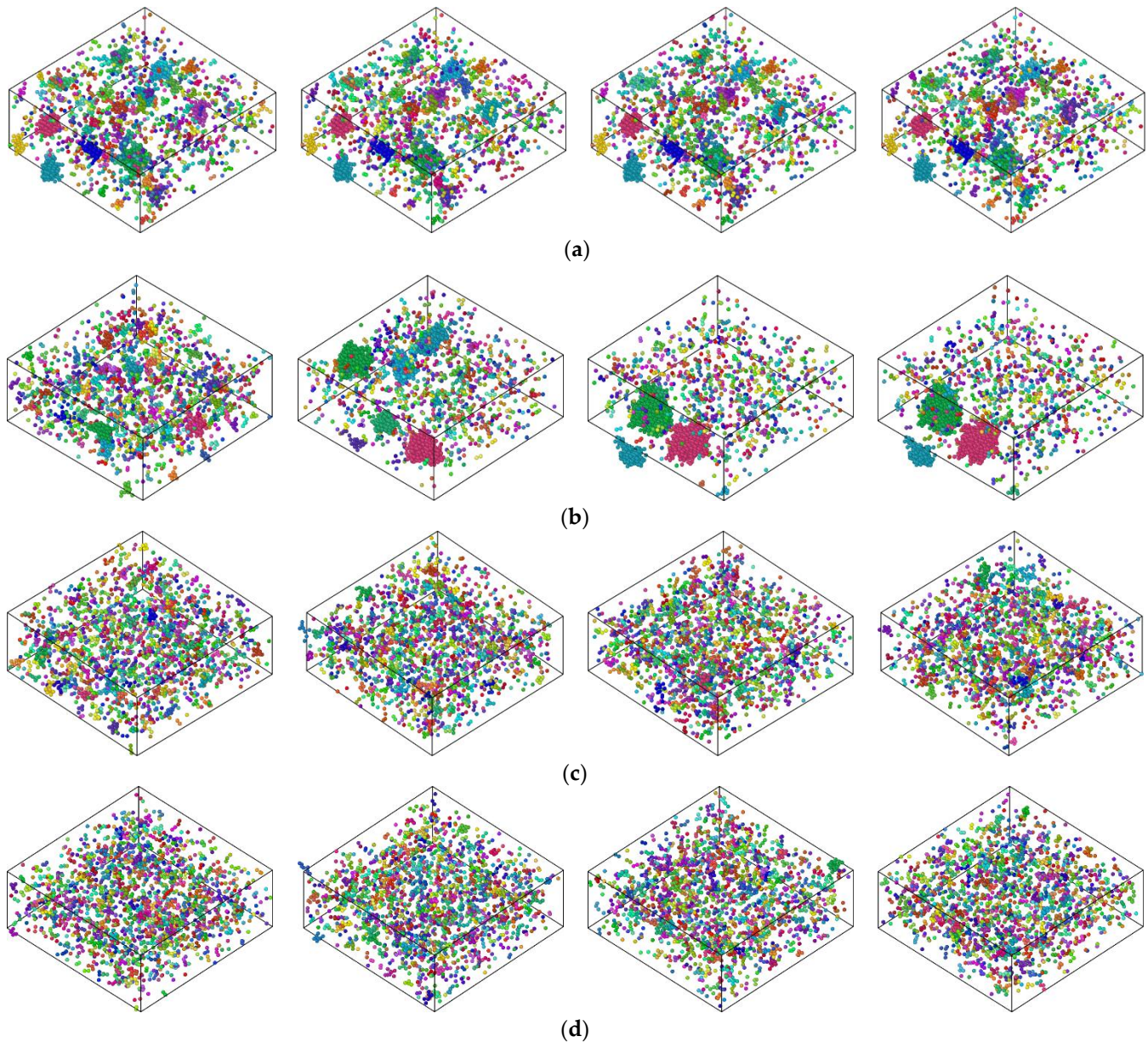


Figure 7. Visualization of Fe atomic distribution states during alloy holding: ((a): 800 K, (b): 1000 K, (c): 1200 K, (d): 1400 K; the four pictures in the horizontal row are the Fe atomic distribution states at 0 ns, 30 ns, 60 ns, and 120 ns, respectively).

During the holding process at a temperature of 800 K, there is essentially no observable change in the atomic distribution of Fe. However, the Fe atoms changed significantly before 60 ns during the holding at 1000 K temperature, and the atoms migrated and aggregated, with small clusters in the initial state, which gradually gathered into large clusters, with small changes in the time range of 60 ns–120 ns. The migration of Fe atoms is clearly

observed when the alloy is held at 1200 K and 1400 K temperature conditions, but the absence of aggregation is not significant. In order to analyze the degree of Fe origin more clearly, the number of Fe atoms contained in the largest Fe clusters and the number of clusters containing more than five atoms in the clusters were plotted versus the holding time under different holding temperature conditions, as shown in Figure 8.

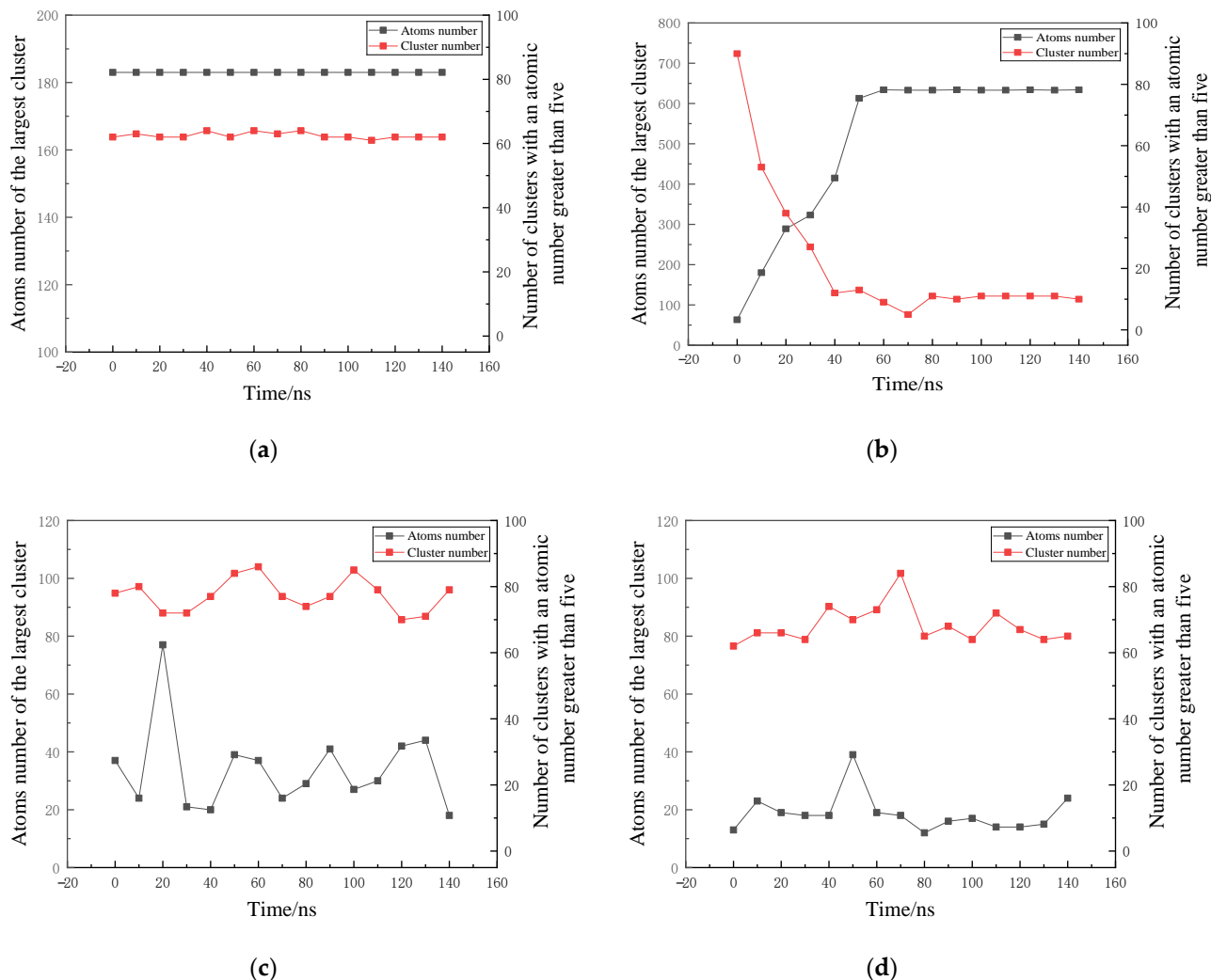


Figure 8. Plot of the number of Fe atoms contained in the largest Fe cluster and the number of clusters containing more than five atoms in the clusters versus the holding time of the alloy at different holding temperatures: ((a): 800 K, (b): 1000 K, (c): 1200 K, (d): 1400 K).

The maximum number of Fe atoms contained in the Fe clusters remained constant at 183 during the holding process of the alloy at 800 K. The number of clusters containing more than five atoms in the clusters did not change much, fluctuating up and down around 62. The number of Fe atoms contained in the largest Fe clusters when the alloy is held at 1000 K increase with the holding time and remain constant until the alloy crystallizes. In contrast, the number of clusters containing more than five atoms decrease with time in the early stage of holding time, and the number of clusters fluctuate after alloy crystallization, but the overall region is stable. From the comparative analysis of the curves in Figure 8b, it can be preliminarily judged that the formation of the largest Fe clusters mainly depends on the continuous migration and condensation of small clusters. Comparing Figure 8c,d, the alloys show an up-and-down trend in the number of Fe atoms contained in the largest Fe cluster and the number of clusters containing more than five atoms in the clusters during

the holding time at 1200 K and 1400 K temperature conditions. There is no single increasing or decreasing trend during the holding time, and the average values of the maximum number of Fe atoms contained in Fe clusters and the number of clusters containing more than five atoms in clusters during the holding time at 1200 K are higher than the values during the holding time at 1400 K. The results show that the alloys are more susceptible to the polymerization of Fe atoms during the holding time at 1200 K. The main reason for this conclusion is that high-temperature molecular thermal motion is intense, the interaction force between Fe atoms is certain, and the higher the temperature, the more uniform the distribution of Fe atoms. To elaborate on the formation process of Fe clusters more clearly, the distribution state of the largest Fe clusters in the alloy at different holding times when the alloy is held at a temperature of 1000 K for 140 ns is derived, as shown in Figure 9, in Figure 9a–i correspond to the holding times of 0 ns, 20 ns, 40.4 ns, 40.889 ns, 41 ns, 41.7 ns, 44 ns, 52.266 ns, and 60 ns.

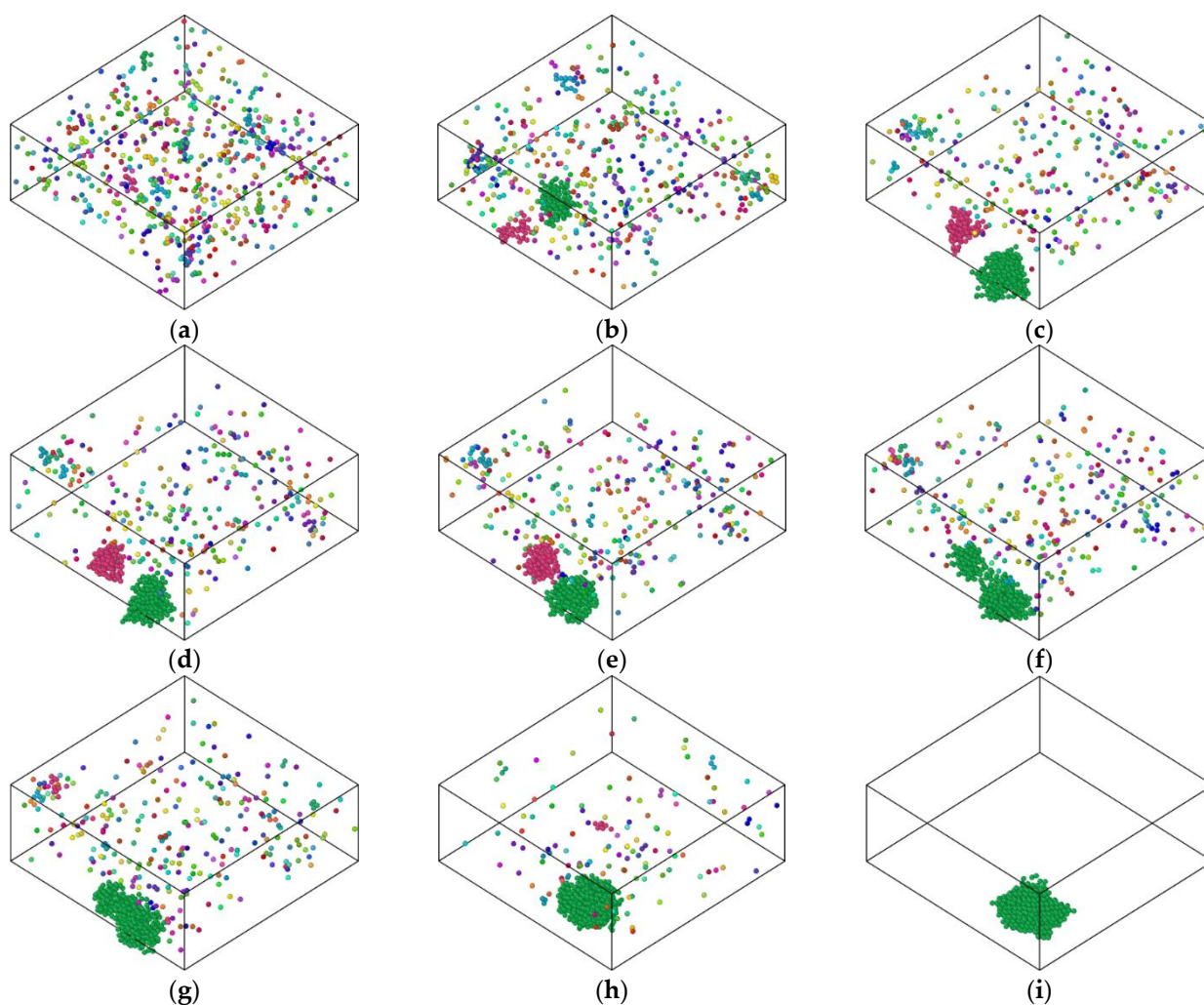


Figure 9. Distribution of maximum Fe clusters at different holding times for the alloy held at 1000 K for 140 ns. ((a): 0 ns, (b): 20 ns, (c): 40.4 ns, (d): 40.889 ns, (e): 41 ns, (f): 41.7 ns, (g): 44 ns, (h):52.266 ns (i): 60 ns).

Figure 9a is the distribution state of Fe atoms at 0 ns of heat preservation. The distribution of atoms in the figure is relatively uniform and only some small clusters. Comparing with the distribution of Fe atoms at 0 ns in Figure 9b, it can be found that the largest Fe clusters are not formed at the beginning, and the original small clusters have been split at a later stage, which is mainly due to the diffusion of Fe atoms caused by

the molecular thermal motion. Comparing Figure 9a–c, aggregation of Fe atoms occurs and nucleation grows. This process is mainly the result of interactions between Fe atoms, where the Fe interatomic interaction forces overcome the molecular thermal motion and aggregation occurs. Figure 9d–f show the process of condensation of two large clusters; this process is mainly the result of the combination of atomic diffusion and interatomic interaction forces, which is the main reason for the change in the curve in Figure 8b. Comparing Figure 9f–i, three changes can be found: One is the gradual aggregation of two large clusters after condensation, which is mainly the role of non-diffusive atomic local structure rearrangement. Secondly, after the large clusters are gathered into one cluster, the morphology of the newly formed cluster gradually changes from irregular shape to spherical shape. The main reason is that the Cu-Fe alloy is a difficult miscible alloy, and there is a large interfacial energy between Cu and Fe. Under the action of interfacial energy, the Fe cluster is gradually spherical. Thirdly, the Fe atoms dispersed in the simulation box are also gradually approaching the Fe clusters, and of course, the Fe atoms have been aggregating to the larger clusters since the beginning. But it is most obvious at this stage, which is the result of atomic diffusion by molecular thermal motion. It is worth noting that the time for Fe atoms to aggregate and form small clusters during the heat preservation process is relatively long, while the condensation time of large clusters is relatively short, which indicates that the mutual attraction of Fe atoms gradually increases after the aggregation of Fe atoms, and the condensation process can be completed in a short period.

4. Conclusions

- (1) Insulation can improve the crystallization point of the alloy. Cu₉₅Fe₅ alloy insulation process atomic potential energy–temperature change line results show that the alloy in the 900 K, 1000 K, and 1100 K temperature conditions when insulation alloy crystallization (normal cold speed conditions alloy crystallization point of 882 K). The lower the holding temperature, the less holding time is required, which indicates that it is easier to crystallize with low-temperature holding.
- (2) The crystalline structure of the alloy is unstable after holding, and some atoms are not in the lattice sites. The alloy is a Cu matrix with a predominantly FCC structure. During the initial stages of crystallization, atom groups with non-FCC structures preferentially crystallize. Subsequent to the holding–cooling process, a redistribution of certain atoms within these non-FCC atom groups occurs, and some atoms become incorporated into the FCC matrix. As a result, the proportion of FCC crystal structure types continues to increase. With the prolongation of the holding–cooling time, the structure of the alloy system is gradually stabilized, and the proportion of each crystal type remains basically unchanged.
- (3) Interaction forces between Fe atoms and molecular thermal motion are important factors affecting the formation of Fe clusters. The analysis of the radial distribution function shows that the Fe atoms of the alloy aggregate under interaction during the insulation at 1000 K and 1100 K. The tendency of aggregation of Fe atoms is weaker under other insulation temperature conditions. The Fe atomic diffusion coefficient was calculated using MSD as a function of holding time. The diffusion coefficient of Fe atoms increases with the increase in the holding temperature, and the diffusion coefficient of Fe atoms is a negative value when the alloy is held at 500 K–900 K, which indicates that the diffusion of Fe atoms in this process is the uphill diffusion, and the diffusion coefficient of Fe atoms is positive under the condition of a holding temperature of more than 900 K.

- (4) The formation of Fe clusters during the insulation process undergoes four main stages. Firstly, the original clusters undergo decomposition, leading to the formation of new clusters as a result of the interplay between molecular thermal motion and the attractive forces among Fe atoms. The second is the condensation and growth of small clusters under the action of non-diffusive atomic localized structural rearrangements. Thirdly, Fe clusters gradually sphericalize under the effect of Cu-Fe interfacial energy. Fourth, individual Fe atoms gradually join large Fe clusters by diffusion

Author Contributions: Y.L.: conception, conceived the research, discussed and commented on the manuscript, funding acquisition. L.L.: writing—original draft, wrote the manuscript, discussed and commented on the manuscript, performed the simulation and analyzed the data. X.W.: conception, writing—original draft, wrote the manuscript, discussed and commented on the manuscript, performed the simulation and analyzed the data. H.Z.: conceived the research, discussed and commented on the manuscript. C.X.: writing—original draft, analyzed the data, discussed and commented on the manuscript. Z.Z.: wrote the manuscript, discussed and commented on the manuscript. X.G.: writing—original draft, analyzed the data, discussed and commented on the manuscript. All authors have read and agreed to the published version of the manuscript.

Funding: This research was funded by National Natural Science Foundation of China (Grant Number 51974129); Hebei Province Graduate Innovation Funding Project (CXZZBS2021100).

Data Availability Statement: The authors confirm that the data supporting the findings of this study are available within the article.

Conflicts of Interest: The authors declare no conflicts of interest that could have appeared to influence the work reported in this paper.

References

1. Yang, K.; Wang, H.; Mo, Y.D.; Lou, H.; Guo, M. Deformation and Precipitation Behavior of Advanced Cu-Fe-(C) Alloys. *Rare Met. Mater. Eng.* **2022**, *51*, 4666–4674.
2. Xu, J.; Guan, B.; Fu, R.; Wu, Y.; Hu, Q.; Zou, J.; Huang, G.; Yan, C. Tailoring the microstructure and mechanical properties of Cu-Fe alloy by varying the rolling path and rolling temperature. *J. Mater. Res. Technol.* **2023**, *27*, 182–193. [[CrossRef](#)]
3. Pang, Y.; Chao, G.; Luan, T.; Gong, S.; Wang, Y.; Jiang, Z.; Xiao, Z.; Jiang, Y.; Li, Z. Microstructure and properties of high strength, high conductivity and magnetic Cu-10Fe-0.4Si alloy. *Mater. Sci. Eng. A* **2021**, *826*, 142012. [[CrossRef](#)]
4. Iwase, A.; Fujimura, Y.; Semboshi, S.; Hori, F.; Matsui, T. Effects of energetic electron irradiation on electric, magnetic, and mechanical properties of Cu-1.2 at.%Fe alloy. *Nucl. Instrum. Methods Phys. Res. Sect. B Beam Interact. Mater. At.* **2024**, *556*, 165506. [[CrossRef](#)]
5. Liu, K.M.; Sheng, X.C.; He, G.Y.; Han, N.L.; Li, M.L.; Zhang, M.C.; Zou, J.; Atrens, A.; Huang, H.M. Microstructure and Electrical Resistivity of In Situ Cu-Fe Microcomposites. *J. Mater. Eng. Perform.* **2022**, *31*, 3896–3901. [[CrossRef](#)]
6. Yue, S.P.; Qu, J.P.; Li, G.L.; Liu, S.C.; Guo, Z.K.; Jie, J.C.; Guo, S.L.; Li, T.J. A comprehensive investigation of carbon micro-alloying on microstructure evolution and properties of metastable immiscible Cu-Fe alloy. *J. Alloys Compd.* **2022**, *921*, 166163. [[CrossRef](#)]
7. Wu, Y.; Zhu, B.; Du, H.; Xia, Z.; Su, J.; Gao, Z. Metastable phase separation kinetics controlled by superheating and undercooling of liquid Fe-Cu peritectic alloys. *J. Alloys Compd.* **2022**, *913*, 165268. [[CrossRef](#)]
8. Yue, X.Y.; Peng, S.Y.; Zhang, X.; He, C.N.; Tian, Y.Z. Distinct Electrical and Mechanical Responses of a Cu-10Fe Composite Prepared by Hot-Pressed Sintering and Post Treatment. *Acta Metall. Sin. (Engl. Lett.)* **2024**, *37*, 255–265. [[CrossRef](#)]
9. Morshed, A.K.M.M.; Shahadat, M.R.B.; Roni, M.R.H.; Masnoon, A.S.; Shamim, S.A.-A.; Paul, T.C. A Molecular Dynamics Study of Heat Transfer Enhancement during Phase Change from a Nanoengineered Solid Surface. *Processes* **2021**, *9*, 715. [[CrossRef](#)]
10. Samiri, A.; Khmich, A.; Hasnaoui, A. Understanding the relationship between structural and dynamic properties in binary Mg-Al metallic liquids from molecular dynamics simulations. *Mater. Today Commun.* **2024**, *41*, 110494. [[CrossRef](#)]
11. Mahata, A. Bridging molecular dynamics and additive manufacturing: A study of Al-12 at% Si alloy solidification dynamics. *Mater. Today Commun.* **2024**, *40*, 109782. [[CrossRef](#)]
12. Wang, X.F.; Gao, X.F.; Jin, Y.X.; Zhang, Z.H.; Lai, Z.B.; Zhang, H.Y.; Li, Y.G. Molecular Dynamics Simulation Research on Fe Atom Precipitation Behaviour of Cu-Fe Alloys during the Rapid Solidification Processes. *Materials* **2024**, *17*, 719. [[CrossRef](#)] [[PubMed](#)]
13. Wang, X.F.; Gao, X.F.; Lai, Z.B.; Han, Z.E.; Li, Y.G. Molecular Dynamics Research on Fe Precipitation Behavior of Cu95Fe5 Alloys during Rapid Cooling. *Metals* **2024**, *14*, 228. [[CrossRef](#)]

14. Hirel, P. AtomsK: A tool for manipulating and converting atomic data files. *Comput. Phys. Commun.* **2015**, *197*, 212–219. [[CrossRef](#)]
15. Plimpton, S. Fast Parallel Algorithms for Short-Range Molecular Dynamics. *J. Comput. Phys.* **1995**, *117*, 1–19. [[CrossRef](#)]
16. Bonny, G.; Pasianot, R.C.; Castin, N.; Malerba, L. Ternary Fe-Cu-Ni many-body potential to model reactor pressure vessel steels: First validation by simulated thermal annealing. *Philos. Mag.* **2009**, *89*, 3531–3546. [[CrossRef](#)]
17. Stukowski, A. Visualization and analysis of atomistic simulation data with ovito—the open visualization tool visualization and analysis of atomistic simulation data with ovito—the open visualization tool. *Model. Simul. Mater. Sci. Eng.* **2019**, *18*, 015012. [[CrossRef](#)]
18. Wang, M.; Huang, X.; Wu, S.; Dai, G. Molecular dynamics simulations of tensile mechanical properties and microstructures of Al-4.5Cu alloy: The role of temperature and strain rate. *Model. Simul. Mater. Sci. Eng.* **2022**, *30*, 04500. [[CrossRef](#)]
19. Cheng, Q.; Chen, L.; Tang, J.; Zhao, G.; Sun, L.; Zhang, C. A comprehensive analysis on microstructure evolution of Mg-5.65Zn-0.66Zr alloy during hot deformation—ScienceDirect. *J. Magnes. Alloys* **2020**, *9*, 520–531. [[CrossRef](#)]
20. Abu-Hamdeh, N.H.; Alsulami, R.A.; Alimoradi, A.; Karimipour, A. Fluid flow and heat transfer of the two-phase solid/liquid mixture at the equilibration phase structure via MD method: Atomic value effects in a case study of energy consumption and absorbed energy. *J. Mol. Liq.* **2021**, *337*, 116384. [[CrossRef](#)]
21. Chalamet, L.; Rodney, D.; Shibuta, Y. Coarse-grained molecular dynamic model for metallic materials. *Comput. Mater. Sci.* **2023**, *228*, 112306. [[CrossRef](#)]
22. Samantaray, M.P.; Sarangi, S.S. Effect of cooling rate on solidification points and atomic structures of metal nanoclusters: A molecular dynamics simulation study. *Phys. Scr.* **2023**, *98*, 125971. [[CrossRef](#)]
23. Wang, N.J.; Zhang, Y.X.; Wang, Y.; Fang, F.; Wu, T.M.; Chen, L.; Kang, J.; Wang, G.D.; Yuan, G. An experimental and molecular dynamics study on the formation of low-energy grain boundaries induced by grain rotation during rapid solidification. *Mater. Lett.* **2023**, *352*, 135116. [[CrossRef](#)]
24. Qin, Q.; Li, W.Z.; Wang, W.R.; Li, D.Y.; Xie, L. Effect of Temperature Gradient and Cooling Rate on the Solidification of Iron: A Molecular Dynamics Study. *Materials* **2024**, *17*, 6051. [[CrossRef](#)] [[PubMed](#)]
25. Nguyen-Trong, D.; Nguyen-Tri, P. Factors affecting the structure, phase transition and crystallization process of AlNi nanoparticles. *J. Alloys Compd.* **2020**, *812*, 152133. [[CrossRef](#)]
26. Tang, J.B.; Ahmadi, A.; Alizadeh, A.; Abedinzadeh, R.; Abed, A.M.; Smaism, G.F.; Hadrawi, S.K.; Nasajpour-Esfahani, N.; Toghraie, D. Investigation of the mechanical properties of different amorphous composites using the molecular dynamics simulation. *J. Mater. Res. Technol.* **2023**, *24*, 1390–1400. [[CrossRef](#)]
27. Liu, W.T.; Peng, J.; Liu, J.J.; Li, J.; Liu, B.; Fang, Q.H. Investigation of the sintering behavior of nanoparticulate SiC by molecular dynamics simulation. *Mater. Today Commun.* **2024**, *41*, 110654. [[CrossRef](#)]
28. Agudelo-Giraldo, J.D.; Cantillo-Galindo, N.; López-Salguero, J.S.; Reyes-Pineda, H. Comparative study of surface disorder in gold and silver nanoparticles obtained by molecular dynamics in cooling processes. *Phys. Scr.* **2023**, *98*, 095407. [[CrossRef](#)]
29. Syarif, J.; Gillette, V.; Hussien, H.A.; Badawy, K.; Jisrawi, N. Molecular dynamics simulation of the amorphization and alloying of a mechanically milled Fe-Cu system. *J. Non-Cryst. Solids* **2022**, *580*, 121410. [[CrossRef](#)]
30. Zhang, S.Z.; Wu, Y.K. Investigating the crystallization behavior of TiO₂ during annealing: Molecular dynamics simulations. *Aip Adv.* **2023**, *13*, 085226. [[CrossRef](#)]
31. Usler, A.L.; Kemp, D.; Bonkowski, A.; De Souza, R.A. A general expression for the statistical error in a diffusion coefficient obtained from a solid-state molecular-dynamics simulation. *J. Comput. Chem.* **2023**, *44*, 1347–1359. [[CrossRef](#)] [[PubMed](#)]

Disclaimer/Publisher’s Note: The statements, opinions and data contained in all publications are solely those of the individual author(s) and contributor(s) and not of MDPI and/or the editor(s). MDPI and/or the editor(s) disclaim responsibility for any injury to people or property resulting from any ideas, methods, instructions or products referred to in the content.